High-frequency intrinsic dynamics of the electrocaloric effect from direct atomistic simulations

S. Lisenkov and I. Ponomareva

Department of Physics, University of South Florida, Tampa, Florida 33620, USA

We propose a computational methodology capable of harvesting isothermal heat and entropy change in molecular dynamics simulations. The methodology is applied to study high-frequency dynamics of the electrocaloric effect (ECE) in ferroelectric PbTiO$_3$. ECE is associated with a reversible change in temperature under adiabatic application of electric field or with a reversible change in entropy under isothermal application of the electric field. Accurate assessment of electrocaloric performance requires the knowledge of three quantities: isothermal heat, isothermal entropy change, and adiabatic temperature change. Our methodology allows computations of *all* these quantities *directly*, that is, without restoring to the reversible thermodynamical models. Consequently, it captures both reversible and irreversible effects, which is critical for ECE simulations. The approach is well suited to address the dynamics of the ECE, which so far remains underexplored. We report the following basic features of the intrinsic dynamics of ECE: (i) the ECE is independent of the electric field frequency, rate of application, or field profile; (ii) the effect persists up to the frequencies associated with the onset of dielectric losses and deteriorates from there due to the creation of irreversible entropy; and (iii) in the vicinity of the phase transition and in the paraelectric phase the onset of irreversible dynamics occurs at lower frequency as compared to the ferroelectric phase. The latter is attributed to lower intrinsic soft-mode frequencies and and larger losses in the paraelectric phase.

I. INTRODUCTION

The electrocaloric effect (ECE) is associated with a reversible change in temperature under adiabatic application of an electric field or with a reversible change in entropy under isothermal application of the electric field. In many cases the effect can be described by the thermodynamical differential relation (Maxwell equation) that predicts the electrocaloric coefficient

$$\frac{dT}{dE} = -\frac{T}{C_E}\left(\frac{\partial P}{\partial T}\right)_E, \qquad (1)$$

where T, E, and P are the temperature, electric field, and the polarization, respectively, while C_E is the heat capacity under constant electric field. The interest in ECE has spiked in the recent years [1–4] following the reports of giant ECE in thin films [5,6] and owing to its potential for solid-state refrigeration [7,8]. The ECE is characterized by three essential parameters: the isothermal heat Q, the isothermal entropy change ΔS, and the adiabatic temperature change ΔT. These quantities can either be measured directly (the direct approach) or can be estimated with the help of Maxwell relations [Eq. (1)] (the indirect approach). The direct approach is highly desirable but also challenging. On the other hand, the indirect approach is rather straightforward but only applicable for nonhysteretic fully reversible processes. Computationally caloric effects can also be studied by using either direct or indirect approaches. In the direct approach an electric field is applied under adiabatic conditions and the associated adiabatic change in temperature is directly computed. This approach can be implemented within either Monte Carlo (MC) [9,10] or molecular dynamics (MD) [11,12] techniques. Success

in the development of atomistic simulations that mimic the direct method [9–11,13,14] has led to many insights into the caloric effects. Some examples include predictions of giant elastocaloric effect in ferroelectric ferroelastics [15] which was later confirmed experimentally [16] and prediction of multicaloric effect in ferroelectric ferroelastics [17] which has also been confirmed experimentally [18]. Despite all these, we are not aware of any computational methodology that allows predictions of other essential electrocaloric metrics: the isothermal heat and entropy change directly.

The dominance of the indirect methods of ECE investigations resulted in the lack of understanding of the ECE under nonequilibrium conditions. One such example is the dynamics of the ECE. It is well known that the response of a material to the electric field in many cases is time/frequency dependent. Such dependence cannot be captured by the Maxwell equation (1). However, this subject is rarely addressed in literature [19]. Does the ECE effect, indeed, have a dynamical component or a frequency dependence? Is there an intrinsic timescale associated with this effect? In the direct computational study of room temperature ECE in Pb(Zr$_{0.4}$Ti$_{0.6}$)O$_3$ bulk and nanodots it was found that under an ac electric field the ECE is independent of the frequency below the resonance frequency of the soft mode [11]. On the other hand, a recent computational study [12] reported that ECE depends on the rate of the electric field application. In particular, the simulations with the electric field turned on or off instantaneously resulted in underestimation of the ECE. Could these studies point to the dependence of the ECE on the electric field evolution? Experimentally, the possible dependence of the ECE on frequency was proposed in a uniaxial organic ferroelectric [20]. The aims of this paper are (i) to propose a computational approach capable of
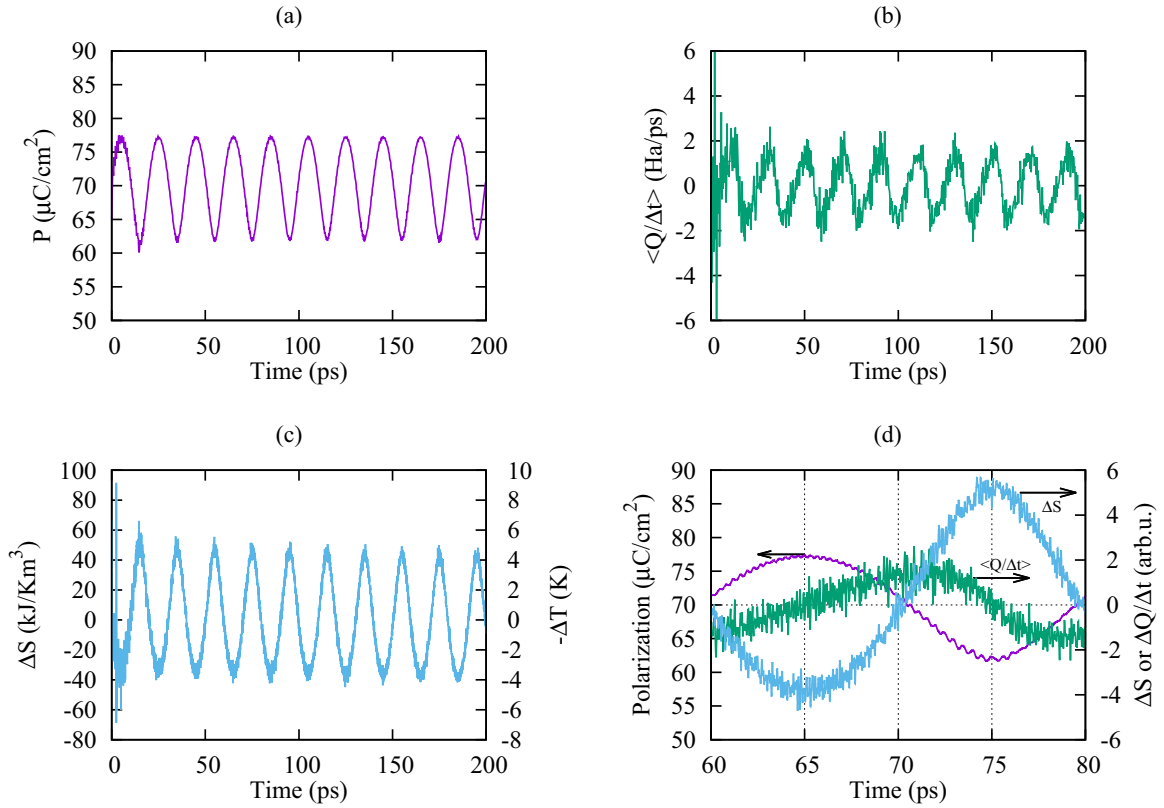
FIG. 1. Room-temperature time evolution of the polarization (a); the average rate of heat exchange (b); isothermal entropy change and adiabatic temperature change (left and right y axis, respectively) (c) under ac electric field; all the above quantities for one period of the field (d).

harvesting isothermal heat and entropy change in MD simulations; (ii) to tailor this approach to simulations of all three essential electrocaloric metrics, namely, Q, ΔS, ΔT, along with their time evolution; and (iii) to apply the methodology to reveal the basic dynamical features of the ECE in ferroelectric PbTiO$_3$.

II. METHODOLOGY

To achieve our methodological goal we use MD with the interactions modeled by the effective Hamiltonian [21]. The degrees of freedom for the effective Hamiltonian include local soft modes, which are proportional to the dipole moment of the unit cell, and strain variables that describe elastic deformation of the unit cell. The interactions between the degrees of freedom in a basic Hamiltonian include a local mode self-energy (harmonic and unharmonic contributions), a long-range dipole-dipole interaction, a short-range interaction between local modes, an elastic energy, the interaction between the local modes and strains, and the interaction of the local modes with the external electric field. For this study we use the effective Hamiltonian for PbTiO$_3$ [21] which was specifically developed to accurately reproduce both static and dynamical properties of this ferroelectric. All interaction parameters for the Hamiltonian are derived from first-principles density functional theory calculations. The Hamiltonian accurately reproduces first-principles ground-state energy, polarization, tetragonality, and soft-mode frequencies. It predicts the

paraelectric to ferroelectric phase transition to occur at 605 K, which underestimates the experimental Curie point of 750 K. Furthermore, it accurately reproduces the frequencies of the soft mode in a wide temperature range. Here we use a simulation supercell of $30 \times 30 \times 30$ perovskite unit cells with periodic boundary conditions applied along all three Cartesian directions to simulate bulk PbTiO$_3$. Using large supercells allows for the reduction of the thermal fluctuations. Some of the simulations were repeated for a $60 \times 60 \times 60$ supercell, however, no significant differences in computational predictions or improvement in thermal fluctuations was found.

In the MD the forces on each degree of freedom is computed from the analytical derivatives of the effective Hamiltonian with respect to its degrees of freedom. The forces are then used in the Newton equations of motion which are integrated numerically using a predictor-corrector algorithm and the integration step of 0.5 fs. To simulate isothermal conditions the supercell is coupled to a thermal bath using the Evans-Hoover approach [22]. The approach introduces an additional frictionlike force $\mathbf{F}_i^{\text{thermo}}$ into the Newton equations of motion that allows for conservation of kinetic energy. The force acts on each site i. The heat that enters/leaves the supercell can be obtained from the energy exchanged with the thermal bath $Q = -\sum_i \mathbf{F}_i^{\text{thermo}} d\mathbf{u}_i$, where $d\mathbf{u}_i$ is the displacement of a degree of freedom. In our case the summation runs over both local modes and local strain variables. The heat is computed at each MD step (the "instantaneous" heat)
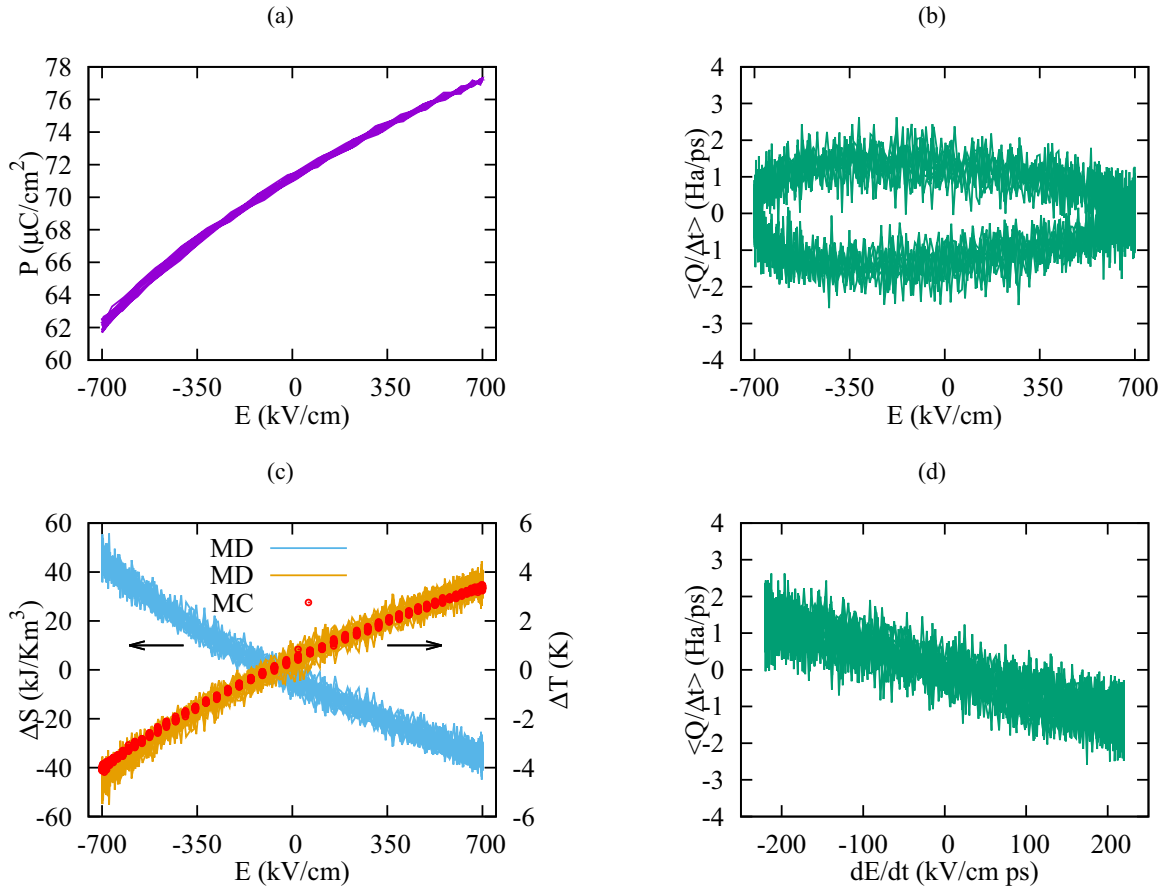
FIG. 2. Room-temperature electric field evolution of the polarization (a); the average rate of heat exchange (b); isothermal entropy change and adiabatic temperature change (left and right y axis, respectively) (c). Solid lines show data obtained from MD calculations, while circles show data from MC simulations. Dependence of the heat exchange rate on the electric field rate (d).

which gives the rate of the heat exchange in isothermal simulations, $Q/\Delta t$, where Δt is the MD time step. The heat is positive if it enters the supercell and negative if it leaves the supercell and contains both reversible and irreversible contributions. The heat can be related to the entropy supplied to (or removed from) the supercell through $\Delta S = Q/T = Q_{rev}/T + Q_{irrev}/T = \Delta S_{rev} + \Delta S_{irrev}$. Here ΔS_{rev} is the reversible entropy change of the supercell, while ΔS_{irrev} is the entropy created through irreversible processes. Similarly, the isothermal heat can be related to the adiabatic change in temperature as $\Delta T = -Q/C = -(Q_{rev} + Q_{irrev})/C = \Delta T_{rev} + \Delta T_{irrev}$, where ΔT_{rev} and ΔT_{irrev} are the reversible and irreversible change in temperature, respectively. Integration of the heat exchange rate over the time gives the net isothermal heat, Q_{net}, entered/left the supercell since the beginning of the simulations. Computationally, this quantity is more convenient to work with since the "instantaneous" Q is rather noisy. Similarly to Q the quantity Q_{net} could be related to the isothermal change in entropy and adiabatic change in temperature. However, these changes are now with respect to their initial values (at the beginning of the simulations). Moreover, for ECE simulations Q_{net} gives the heat exchanged during the field changing from 0 to the current value E, while Q gives the heat exchanged during the field changing from E to $E + \Delta E$, that

is, during one MD step. Note that the computational approach to obtain Q, ΔS, and ΔT is general and independent of the specific force field. It can be applied to harvest isothermal heat and entropy change in any other system.

To simulate the ECE directly, a time-dependent electric field is applied during the simulations and the time evolution of the polarization and isothermal heat are computed. The latter one is converted to heat exchange rate and integrated to obtain isothermal net heat. In this work we consider two different time-dependent electric fields: ac electric field and square-wave electric field. The latter one is often used in direct measurements of the ECE [23–25]. Note that prior to the electric field application the supercell is equilibrated at the desired temperature during 50 ps of isothermal simulations. Therefore, ΔS and ΔT computed from Q_{net} are with respect to their equilibrium values at a given temperature. To reveal the intrinsic dynamics of the ECE we focus on the gigahertz-terahertz frequency range since this range is associated with the intrinsic dynamics of the polar modes which are primary contributors to the ECE. In other words, we do not expect any intrinsic dynamical features below these frequencies. Moreover, focusing on high frequencies allows for establishment of the intrinsic limit for the ECE. While at present the gigahertz-terahertz frequency range is above the range of practical utility
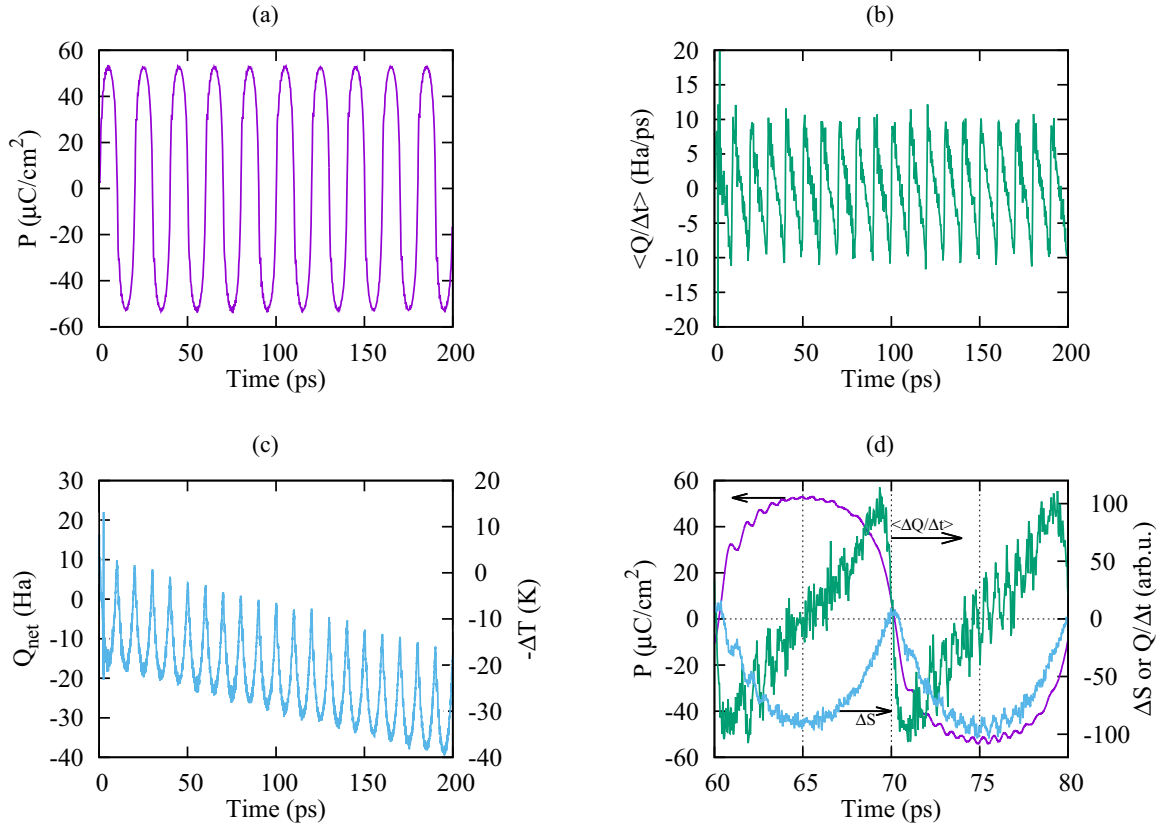
FIG. 3. Time evolution of the polarization (a); the average rate of heat exchange (b); net heat exchanged with the thermal bath (c); time evolution of polarization (left y axis), the average rate of heat exchange (right y axis), and the entropy change (right y axis) during one period of an ac electric field (d). The data were obtained at 700 K.

for macroscopic cooling applications, it could potentially be highly relevant for other applications of ECE, such as temperature-mediated magnetoelectric coupling [26,27].

III. RESULTS AND DISCUSSION

We begin by presenting our room-temperature data for the ac electric field. At room temperature the supercell is polarized along the $\langle 001 \rangle$ direction (positive direction of the z Cartesian axis in our setup). An ac electric field of 700 kV/cm amplitude and 0.05 THz frequency is applied along the direction of the polarization. Figure 1(a) gives the time evolution of the polarization. In this case the polarization follows the time evolution of the electric field. Figure 1(b) gives the average heat exchange rate $\langle Q/\Delta t \rangle$ as a function of time. We used a moving average technique with the averaging interval of 2000 MD steps to compute the average. The computational data for $Q/\Delta t$ are integrated over time to obtain the isothermal net heat Q_{net}, which is then used to compute the isothermal entropy change and the adiabatic temperature change reported on the left and right y axis of Fig. 1(c), respectively. Note that ΔS and ΔT are with respect to their equilibrium values at room temperature. We used the experimental specific heat value from Ref. [28]. In particular, the values of 115 and 144 J/mol K were employed for 300 and 700 K calculations, respectively. From the figure we can see that after the initial transient period the system exhibits steady-state oscillations in

response to the driving field. Figure 1(d) shows the same data as in Figs. 1(a)–1(c) but for one period of oscillations. We can see that the increase in the polarization (first and fourth quarters of the period) is associated with negative $\langle Q/\Delta t \rangle$, that is, heat release to the thermal bath. On the other hand, the decrease in the polarization (second and third quarters of the period) results in positive $\langle Q/\Delta t \rangle$ indicating that the heat is absorbed from the thermal bath. The isothermal entropy evolution (blue line) is opposite to the polarization evolution. In particular, the regions of the polarization increase (the first and last quarters of the period) are associated with the decrease in the ΔS as the electric field aligns the dipoles. On the other hand, the regions where the polarization decreases (second and third quarters of the period) are associated with the increase in the isothermal ΔS. The data presented in Fig. 1 demonstrate the possibility to compute the isothermal heat and entropy change as well as the adiabatic temperature change dynamically. Furthermore, they indicate the existence of the ECE under application of high-frequency ac electric field in agreement with an earlier MD study [11].

Next we investigate the electric field dependence of the quantities given in Fig. 1. The first transient period was removed from the data. Figure 2(a) reports the change in polarization as a function of the electric field, while Figure 2(b) reports the heat exchange rate as a function of the electric field. Interestingly, there exists a hysteresis in $\langle \frac{Q}{\Delta t} \rangle(E)$. To understand the origin of this we write the heat exchange
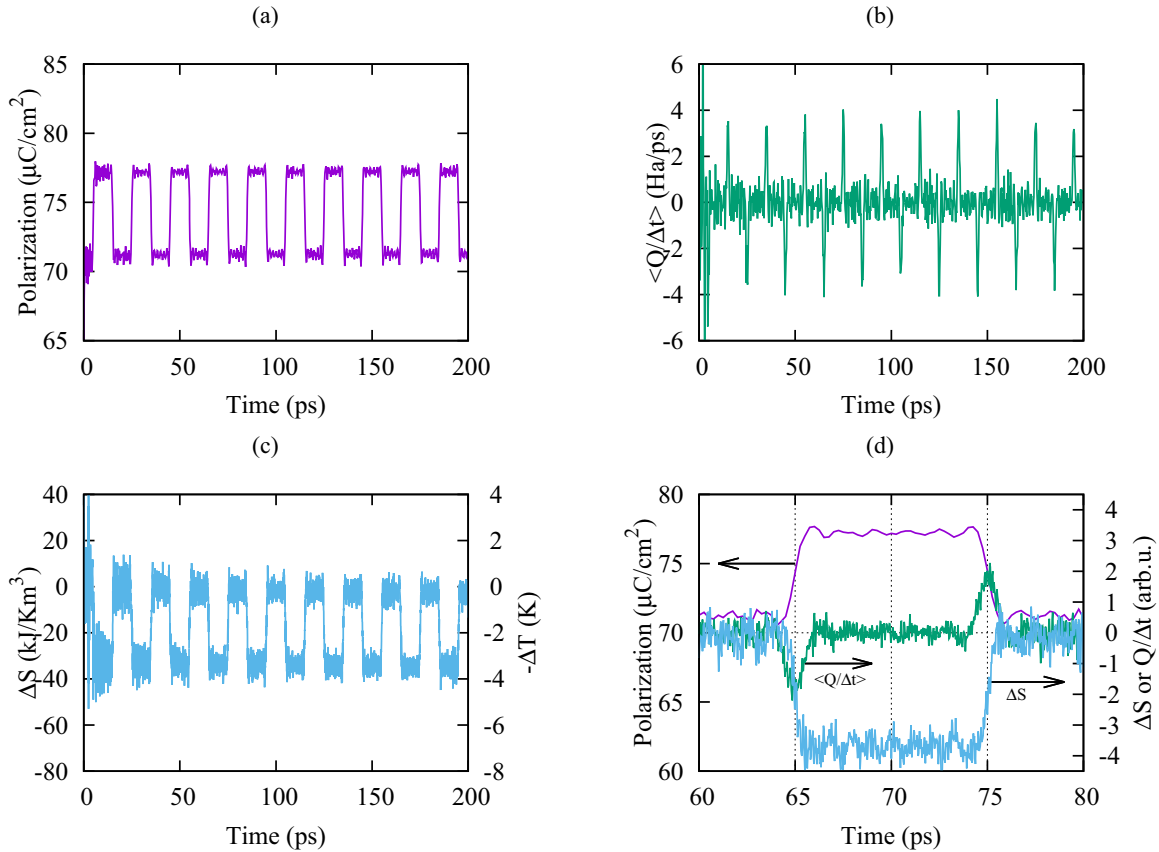
FIG. 4. Room-temperature time evolution of the polarization (a); the average rate of heat exchange (b); isothermal entropy change and adiabatic temperature change (c) (left and right y axis, respectively); all the above quantities for one period of step-like electric field (d).

rate for a reversible isothermal process $(\frac{\partial Q}{\partial t})_T = T(\frac{\partial S}{\partial t})_T = T(\frac{\partial S}{\partial E})_T(\frac{\partial E}{\partial t})_T$. It follows that the rate of the heat exchange is proportional to the rate of the electric field change. The dependence of the rate of the heat exchange on the rate of the electric field application is given in Fig. 2(d). The numerical data confirm that the two rates are directly proportional. Interestingly, the coefficient of proportionality between the rates gives $T(\frac{\partial S}{\partial E})_T$. The linear fit to the data yields the value of -0.57 mJ/(K V m^2) for $(\frac{\partial S}{\partial E})_T$ which falls within the range of experimental data [1]. Figure 2(c) gives the change in isothermal entropy as a function of the electric field (left y axis) and the adiabatic change in temperature as a function of the electric field (right y axis). Technically, both quantities are those obtained from Q_{net} since Q_{net} is a function of the electric field, while $Q/\Delta t$ is a function of the electric field rate. We have also computed the adiabatic ΔT using the semi-classical adiabatic MC that incorporates quantum-mechanical dependence of the heat capacity on temperature [29]. The data are given by the circles on the right y axis in Fig. 2(c). A comparison indicates excellent agreement between the data and confirms the accuracy of our computational methodology. Furthermore, the agreement between the quasistatic (MC) and dynamic (MD) simulations indicates that the intrinsic ECE is independent of the frequency and, therefore, does not have a dynamical component.

We have repeated simulations for a much higher frequency of 0.5 THz. For the electric field amplitude 700 kV/cm the polarization reverses under this field resulting in a irreversible heat loss. Decreasing the amplitude of the ac field down to 500 kV/cm allowed for data collection. The results for $P(E)$, $\langle\frac{Q}{dt}(E)\rangle$, $\Delta S(E)$, and $\Delta T(E)$ overlap with those shown in Fig. 2 in the common field range. This suggests that at room temperature ECE could persist up to very high frequencies and further confirms its independence on frequency.

We have repeated the simulation for the temperature 700 K, which is about 100 K above the computational Curie point of PbTiO$_3$. The electric field of 700 kV/cm amplitude and 0.05 THz frequency was applied along the $\langle 001\rangle$ crystallographic direction. The polarization as a function of temperature is given in Fig. 3(a). The isothermal heat exchange rate is displayed in Fig. 3(b), while the isothermal heat Q_{net} is given in Fig. 3(c). Interestingly, in this case we find a net decrease of Q_{net}, which indicates that the irreversible entropy generated in the supercell is being removed through the heat exchange with the thermal bath. Since we are only interested in the reversible change in entropy we do not convert heat to the entropy change in this case. On the other hand, conversion of the heat to the adiabatic temperature change allows estimation of the irreversible temperature increase and is shown on the right y axis of Fig. 3(c). In this case our calculations predict that under adiabatic conditions the average temperature of the supercell would increase rapidly and irreversibly by about 30 K after 200 ps of field application. To understand the origin of the irreversibility we turn to the intrinsic dynamics of the soft
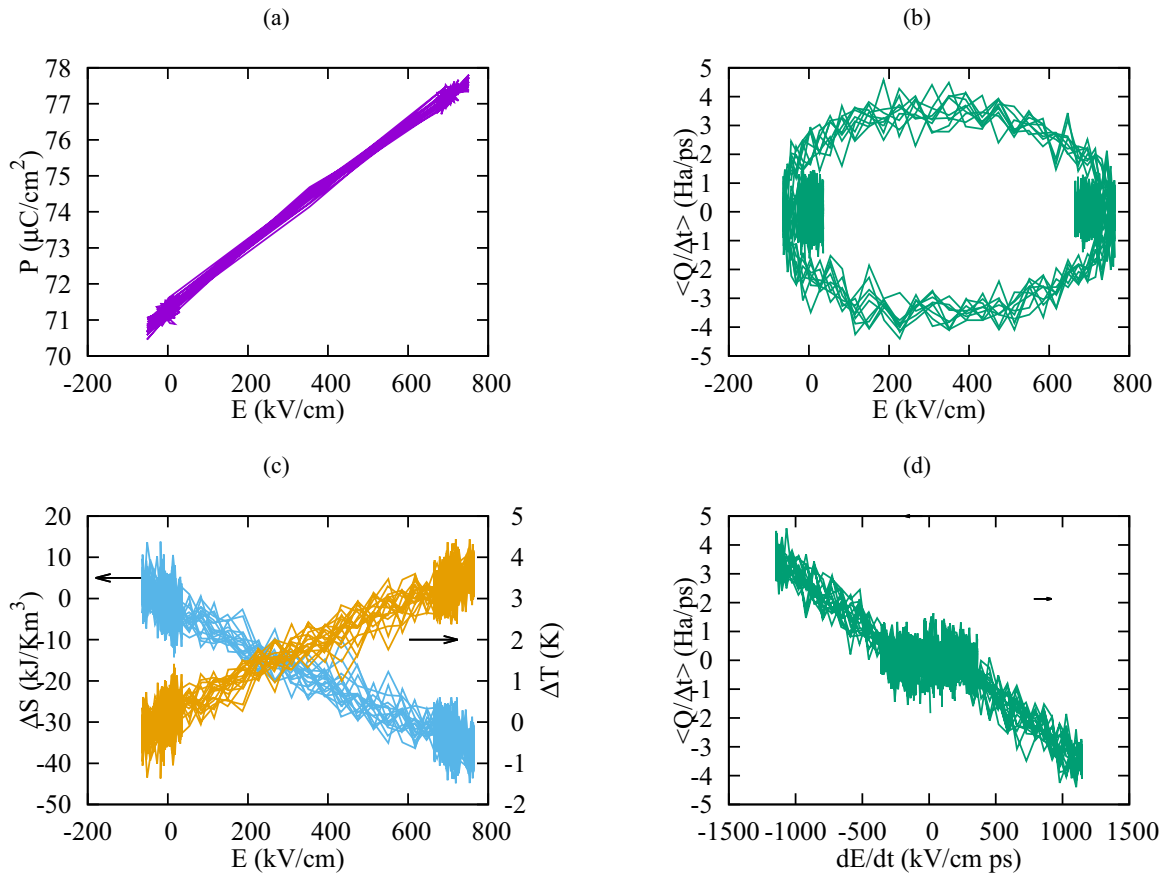
FIG. 5. Room-temperature electric field evolution of the polarization (a); the average rate of heat exchange (b); isothermal entropy change and adiabatic temperature change (c) (left and right y axis, respectively). Dependence of the heat exchange rate on the electric field rate (d).

mode in PbTiO$_3$ [21]. On approaching the phase transition the intrinsic soft-mode frequency decreases significantly while losses (quantified by the damping constant in the harmonic oscillator model) increase drastically [21]. This causes a significant broadening of the imaginary part of the dielectric susceptibility with its peak moving toward lower frequencies. Since it is the imaginary part of the dielectric susceptibility that gives rise to the dielectric losses we find irreversibly close to the phase transition. Interestingly, in Ref. [21] it was found that in the paraelectric phase the damping constant is nearly independent of the temperature. This suggests that the irreversibility would persist in the paraelectric phase even as we move away from the phase transition. To verify this we repeated simulations for 900 K which is 200 K higher than the computational Curie point. In this case we still find that the irreversible heat is generated during the electric field application although less in quantity than at 700 K. This confirms that the irreversibility and associated deterioration of the electrocaloric response in the paraelectric phase originates from the higher dielectric losses. Interestingly, as per finding of Ref. [21] in the ferroelectric phase of PbTiO$_3$ the A$_1$(TO1) mode has much lower losses than the E mode, which suggests that it may be advantageous to apply an electric field along the polar directions in the ferroelectric phase to minimize irreversible heating in high-frequency applications. Figure 3(d) shows the same data as Figs. 3(a) and 3(b) but for one period of the electric field. Since during one period of the electric

field the effects due to irreversibility are small, we convert Q_{net} into the entropy change and add it to Fig. 3(d). In the first quarter of the period the electric field aligns the dipoles along the positive z direction which results in a decrease in the configurational entropy and ejection of the associated heat to the thermal bath. During the second quarter the field decreases back to zero causing the dipoles to lose their ordering and resulting in the increase in configurational entropy and heat absorption from the thermal bath. The situation is identical for the third and fourth quarters of the period as the field aligns and releases the dipoles along the negative direction of the z axis.

Experimentally, direct measurements of ECE are often done using differential scanning calorimetry [23–25]. In such technique the sample is typically subjected to steplike periodic electric field pulses under isothermal conditions. More precisely, the field is first turned on quickly causing the sample's temperature to increase under nearly adiabatic conditions. After that the field is kept on while the sample thermalizes and returns back to the initial temperature. Next the field is removed, quickly causing the sample temperature to drop below the temperature of the thermal bath. Finally, as the field remains off, the sample returns to the original temperature. Perhaps, one of the stringent tests to our computational methodology would be the ability to simulate such experiments. Motivated to address this, we simulate the ECE under isothermal application of a steplike periodic electric field (square wave) at 300 K. The field was simulated by using the first six terms of the

Fourier series expansion of a square wave: $E = E_0(1/2 + 2/\pi)\sum_{k=1}^{6}\sin[(2k-1)\omega t + 3\pi/2]/(2k-1)$, where E_0 and ω are the square-wave amplitude and frequency, respectively. In these settings the minimum and maximum field is 0 and E_0, respectively, which simulates field's "off" and "on" phases. Note that we avoided using higher harmonics in the expansion due to their proximity to the intrinsic soft-mode frequency. We used $E_0 = 700$ kV/cm and $\omega/2\pi = 0.05$ THz. Figure 4(a) shows the response of the polarization to the field, while Fig. 4(b) shows the average heat exchange rate. The latter resemble closely the experimental data from differential scanning calorimetry [23,24]. The negative spikes are associated with turning the field "on," while positive spikes occur when the field is turned "off." Figure 4(c) shows the isothermal entropy change (left y axis) and adiabatic temperature change (right y axis) with respect to their equilibrium values. These quantities show steplike evolution as well. Figure 4(d) displays the data for one period of the electric field. We can see that the rapid increase in the polarization results in the dip in the heat exchange rate, while a subsequent rapid decrease in the polarization leads to the symmetric peak in the heat exchange rate. The isothermal entropy decreases as the polarization increases, owing to the alignment of the dipoles by the field, and then returns to the original value as the field is removed.

To gain further insight we plot the field dependence of the polarization, heat exchange rate, and adiabatic heat in Figs. 5(a)–5(c). Note that the first transient period has been removed. A comparison between Figs. 2 and 5 shows the agreement between the data for the $P(E)$, $\Delta S(E)$, and $\Delta T(E)$ for the common range of the electric field. The agreement between the data for the ac and square-wave electric fields indicates that the ECE is independent of the electric field profile. Figure 5(b) shows once again that the heat exchange rate exhibits hysteresis when plotted as a function of the electric field. On the other hand, the hysteresis is removed when $Q/\Delta t$ is plotted as a function of the electric field application rate [Fig. 5(d)]. Simulations at 700 and 900 K resulted in the same outcome as for the ac electric field. Namely, the presence of irreversible heat. This suggests that the application of periodic fields in the gigahertz-terahertz frequency range is not feasible in the paraelectric phase of ferroelectrics for caloric effect applications. On the other hand, application of the field along the polar direction of ferroelectrics allows one to overcome this limitation.

IV. CONCLUSIONS

In summary, we have proposed a computational methodology that allows harvesting of heat and entropy change during isothermal MD simulations. The methodology is well suited for direct simulations of the ECE and allows for computations of three essential electrocaloric metrics: isothermal heat and entropy change, and adiabatic temperature change. Application of the methodology to study high-frequency dynamics in ferroelectric $PbTiO_3$ revealed that the ECE persists up to the frequencies associated with the onset of dielectric losses which result in the irreversible heat creation. At that point the electrocaloric properties deteriorate due to the irreversible entropy generation. As these frequencies depend strongly on the temperature the intrinsic limit for the ECE is also temperature dependent. In particular, in the paraelectric phase and in the vicinity of the phase transition in $PbTiO_3$ we find irreversible heat for the ac field frequency of 0.05 THz. On the other hand, application of the same electric field in the ferroelectric phase along the polar direction is completely reversible. Application of the square-wave electric field revealed that our methodology is capable of simulating differential scanning calorimetry experiments. We found no differences between the electrocaloric metrics from the simulations under the ac and square-wave electric field, which suggests that the ECE is independent of the electric field profile or its rate of application. We also report that the heat exchange rate (or electrocaloric power) is proportional to the rate of the electric field application. Therefore, optimization of the heat exchange rate can be achieved through optimization of the time evolution of the electric field.

[1] S. Crossley, N. D. Mathur, and X. Moya, AIP Adv. **5**, 067153 (2015).

[2] S.-G. Lu and Q. Zhang, Adv. Mater. **21**, 1983 (2009).

[3] *Electrocaloric Materials: New Generation of Coolers*, edited by T. Correia and Q. Zhang (Springer, Berlin/Heidelberg, 2014).

[4] J. F. Scott, Ann. Rev. Mater. Sci. **41**, 229 (2011).

[5] A. Mischenko, Q. Zhang, J. Scott, R. Whatmore, and N. Mathur, Science **311**, 1270 (2006).

[6] B. Neese, B. Chu, S.-G. Lu, Y. Wang, E. Furman, and Q. M. Zhang, Science **321**, 821 (2008).

[7] P. Blumenthal and A. Raatz, Europhys. Lett. **115**, 17004 (2016).

[8] S. Fahler, U. K. Robler, O. Kastner, J. Eckert, G. Eggeler, H. Emmerich, P. Entel, S. Muller, E. Quandt, and K. Albe, Adv. Eng. Mater. **14**, 10 (2012).

[9] S. Lisenkov and I. Ponomareva, Phys. Rev. B **80**, 140102 (2009).

[10] I. Ponomareva and S. Lisenkov, Phys. Rev. Lett. **108**, 167604 (2012).

[11] S. Prosandeev, I. Ponomareva, and L. Bellaiche, Phys. Rev. B **78**, 052103 (2008).

[12] M. Marathe, A. Grünebohm, T. Nishimatsu, P. Entel, and C. Ederer, Phys. Rev. B **93**, 054110 (2016).

[13] T. Nishimatsu, J. A. Barr, and S. P. Beckman, J. Phys. Soc. Jpn. **82**, 114605 (2013).

[14] S. Lisenkov, R. Herchig, S. Patel, R. Vaish, J. Cuozzo, and I. Ponomareva, Nano Lett. **16**, 7008 (2016).

[15] S. Lisenkov and I. Ponomareva, Phys. Rev. B **86**, 104103 (2012).

[16] A. Chauhan, S. Patel, and R. Vaish, Appl. Phys. Lett. **106**, 172901 (2015).

[17] S. Lisenkov, B. K. Mani, C.-M. Chang, J. Almand, and I. Ponomareva, Phys. Rev. B **87**, 224101 (2013).

[18] A. Chauhan, S. Patel, and R. Vaish, Acta Mater. **89**, 384 (2015).

[19] Y. Liu, J. F. Scott, and B. Dkhil, Appl. Phys. Rev. **3**, 031102 (2016).

[20] S. E. Rowley, M. Hadjimichael, M. N. Ali, Y. C. Durmaz, J. C. Lashley, R. J. Cava, and J. F. Scott, J. Phys.: Condens. Matter **27**, 395901 (2015).

[21] B. K. Mani, C.-M. Chang, and I. Ponomareva, Phys. Rev. B **88**, 064306 (2013).

[22] D. Rapaport, *The Art of Molecular Dynamics Simulation* (Cambridge University Press, Cambridge, 1997).

[23] M. Sanlialp, C. Molin, V. V. Shvartsman, S. Gebhardt, and D. C. Lupascu, IEEE Trans. Ultrason. Ferroelectr. Freq. Control **63**, 1690 (2016).

[24] D. Guyomar, G. Sebald, B. Guiffard, and L. Seveyrat, J. Phys. D **39**, 4491 (2006).

[25] Z. Kutnjak and B. Rožič, in *Electrocaloric Materials: New Generation of Coolers*, edited by T. Correia and Q. Zhang (Springer, Berlin/Heidelberg, 2014), pp. 147–182.

[26] C.-M. Chang, B. K. Mani, S. Lisenkov, and I. Ponomareva, Phys. Rev. Lett. **114**, 177205 (2015).

[27] R. Herchig, J. Cuozzo, S. Lisenkov, and I. Ponomareva, Appl. Phys. Lett. **111**, 152904 (2017).

[28] G. A. Rossetti and N. Maffei, J. Phys.: Condens. Matter **17**, 3953 (2005).

[29] P. Jouzdani, S. Cuozzo, S. Lisenkov, and I. Ponomareva, Phys. Rev. B **96**, 214107 (2017).